

Validation of the influence of CT slice thickness on the quantitative accuracy and image quality of single photon emission computed tomography

Tomohiro Sato*, Takashi Takagi

Department of Radiology, Chiba Aoba Municipal Hospital, Chiba City, Japan

ARTICLE INFO

Article type:
Original Article

Article history:
Received: 12 Jan 2021
Revised: 27 Apr 2021
Accepted: 10 May 2021

Keywords:
SPECT/CT
Radiation dose
CT slice thickness
Image quality
OSCGM

ABSTRACT

Objective(s): Computed tomography (CT) images are used for precise anatomical location of lesions and for accurate attenuation correction in single-photon emission computed tomography (SPECT) image reconstruction in SPECT/CT examination. The aim of this study was to verify the effects of varying CT collimation width and slice thickness on CT images and on CT attenuation corrected SPECT images.

Methods: We acquired SPECT/CT images of a micro-coin phantom and the National Electrical Manufacturers Association body phantom filled with ^{99m}Tc -pertechnetate while varying the abovementioned CT parameters. The full width at half maximum of the slice sensitivity profile, the standard deviation of CT image background noise, and the radiation dose from CT scans were evaluated. Subsequently, the percentage contrast, background variability, and absolute recovery coefficient of the SPECT image were measured. Furthermore, we retrospectively reviewed the clinical bone SPECT images of 23 patients, and statistical testing of differences was performed.

Results: As the collimation width and reconstruction slice thickness of the CT image increased, z-axis resolution deteriorated, and background noise decreased. In addition, CT radiation dose decreased with increasing collimation width. Meanwhile, SPECT image quality and quantitative accuracy were unchanged with varying CT collimation width and slice thickness. There were no notable variations in clinical SPECT images and no statistically significant differences.

Conclusion: When high-resolution CT slices on the z-axis are not required for clinical diagnosis, increasing collimation width or slice thickness can reduce the radiation dose and image noise with no influence on the quality of SPECT images.

► Please cite this paper as:

Sato T, Takagi T. Validation of the influence of CT slice thickness on the quantitative accuracy and image quality of single photon emission computed tomography. *Asia Ocean J Nucl Med Biol.* 2021; 9(2): 148-157. doi: 10.22038/AOJNMB.2021.54670.1376

Introduction

The standardized uptake value (SUV) has been widely used in positron emission tomography (PET) and is the quantitative index conventionally used for the measurement of objective radiotracer uptake in tissues and for the assessment of cell metabolism (1). In recent years, quantitative single-photon emission computed tomography (SPECT) has been developed and clinically applied with the advent

of SPECT/computed tomography (CT), advances in algorithms for image reconstruction, and correction techniques for photon attenuation and scattering (2). Quantitative bone SUV has been reported as a useful prognostic indicator of bone metastases and improves its differentiation from degenerative changes in patients with prostate cancer (3).

The CT images are used for accurate attenuation correction in SPECT and PET image

* Corresponding author: Tomohiro Sato. Department of Radiology, Chiba Aoba Municipal Hospital, 1273-2 Aoba-cho, Chuoku, Chiba City, Chiba 260-0852, Japan. Tel: +81432271131; Fax: +81432272022; Email: tomohiro.satou@jade.plala.or.jp
© 2021 *mums.ac.ir* All rights reserved.

This is an Open Access article distributed under the terms of the Creative Commons Attribution License (<http://creativecommons.org/licenses/by/3.0>), which permits unrestricted use, distribution, and reproduction in any medium, provided the original work is properly cited.

reconstruction by converting the CT value into the linear attenuation coefficient of the γ -rays (4, 5). In addition, SPECT/CT fused images enable functional verification of lesions found on SPECT imaging and the precise anatomical location of lesions detected by CT. Such fusion of functional and structural examinations lessens diagnostic difficulties resulting from the interpretation of a single modality. It has been confirmed that SPECT/CT fusion imaging using technetium-99m-methoxyisobutylisonitrile (^{99m}Tc -MIBI) is a more useful tool for the localization of parathyroid lesions, particularly parathyroid adenomas, compared with planar and SPECT imaging (6).

Although the CT image used for attenuation correction in the conventional image reconstruction method is down-sampled to the voxel size of the SPECT image. However, a novel image reconstruction method (xSPECT; Siemens Healthcare, Knoxville, TN, USA) has enabled the acquisition of high-resolution SPECT images by arranging SPECT images according to the CT coordinate system with high accuracy. This method incorporates attenuation correction that maintains the detailed anatomical information of CT and utilizes an ordered-subset conjugate gradient minimization (OSCGM) algorithm suitable for processing large amounts of data (7).

The high-resolution image reconstruction method that arranges SPECT images according to the CT coordinate system is suspected to be easily influenced by the CT parameters. It has been confirmed that differences in the field of view (FOV) of CT do not affect SPECT images (8), but no study has investigated differences in the collimation width and slice thickness of CT.

Therefore, the aim of this study was to verify the effects of varying CT collimation width and slice thickness on CT images and on CT attenuation corrected SPECT images with the OSCGM reconstruction method.

Methods

Phantom studies

CT phantom studies were performed using a dual-head SPECT system (Symbia Intevo 6; Siemens Healthcare, Knoxville, TN, USA), which

performs CT scanning with a maximum of 6 slice acquisitions per rotation and Syngo MI Applications VB20 software (Siemens Healthcare). To measure the slice thickness of CT images, a micro-coin phantom (Kyoto Kagaku Co., Ltd., Kyoto, Japan) was placed 20 mm below the center of the FOV (9), and CT scans were acquired with a tube voltage of 130 kVp routinely used for Clinical SPECT/CT, gantry rotation time of 0.6 s, tube current–exposure time product of 72 mAs, pitch factor of 1.8 (40 effective mAs), and FOV of 500 mm. Collimation was set to 6×1.0 , 2.0, and 3.0, respectively. Effective mAs was set close to the CT dose described for clinical cases in Section 2.3.

CT data were reconstructed with a display FOV of 50 mm, using a filter kernel (B31s medium smooth). Slice thickness was set to 1.25, 2.5, 3.0, 4.0, 5.0, 6.0, 8.0, and 10.0 mm and slice spacing was set to 0.2 mm. An outline drawing of the micro-coin phantom is shown in Figure 1a.

SPECT/CT phantom studies were performed using the same integrated SPECT/CT system as above, in accordance with the Japanese guidelines on standardization of bone SPECT imaging. The National Electrical Manufacturers Association (NEMA) body phantom (Kyoto Kagaku Co., Ltd.) was filled with ^{99m}Tc -pertechnetate, which was mixed thoroughly prior to imaging. Six spheres with diameters of 10, 13, 17, 22, 28, and 37 mm which have radioactivity concentration of 106.5 kBq/ml were obtained from the phantom, while background (BG) activity was 17.7 kBq/ml, with a hot sphere-to-BG ratio of 6:1 (10). An outline drawing of the NEMA body phantom is shown in Figure 1b. A radioisotope dose calibrator (CRC-55t; Capintec, Florham Park, NJ, USA) was used to measure radioactivity. SPECT scans were acquired using low-energy high-resolution collimation, a 256×256 matrix of 2.4-mm pixels and a total of 120 projections over 360° in a body-contour orbit with a dwell time of 15 s/view. The energy windows were set at 140.0 keV $\pm 7.5\%$ and 118 keV $\pm 7.5\%$. After the SPECT acquisition, CT scans were acquired with a 500-mm FOV; all other parameters were the same as in the CT phantom studies. Collimation was set to 6×1.0 , 2.0, and 3.0.

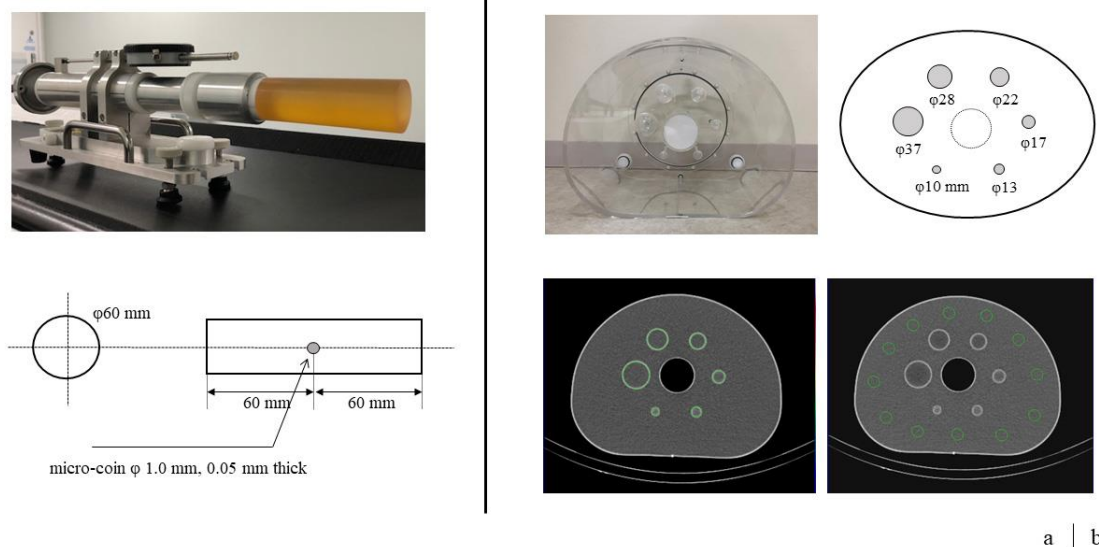


Figure 1. (a) Micro-coin phantom consisting of a polyurethane cylinder and tungsten disc. (b) NEMA body phantom (top); ROIs were drawn on each sphere and the background of the SPECT, the CT, and the μ -map images (bottom)

SPECT reconstructions were performed using OSCGM, the image reconstruction algorithm used for xSPECT (Siemens Healthcare) with scatter correction using a dual-energy window approach, attenuation correction based on a CT-derived attenuation map (μ -map), and depth-dependent spatial resolution correction using a point-spread response function. The reconstruction parameter for “Exam Type” was set to “Skeletal,” with 1 subset and 48 iterations and a Gaussian filter with a full width at half maximum (FWHM) of 10.0 mm, without zone-map enhancement. The FWHM of the Gaussian filter and the subset and iterations were set automatically from the total count of the projection data with a parameter setting of “Standard”. The pixels and slice thickness were automatically set to 1.95 mm, which was an integer multiple of the CT pixel size and the closest value to the pixel size of SPECT acquisition. Furthermore, a μ -map representing the linear attenuation coefficient of the γ -rays was obtained by converting from the CT value in the image reconstruction. The pixels and slice thickness of μ -map were also set to 1.95 mm, the same as in the SPECT reconstruction.

CT data were reconstructed using a filter kernel (B31s medium smooth). Slice thickness was changed to 1.25, 2.5, 4.0, 8.0, and 10.0 mm for a collimation width of 1.0 mm; 2.5, 4.0, 8.0, and 10.0 mm for a collimation width of 2.0 mm; and 4.0, 8.0, and 10.0 mm for a collimation width of 3.0 mm. The slice gap was set to the same value as the slice thickness.

The SPECT/CT system was calibrated using a quantification application (Broad Quantification; Siemens Healthcare) to derive the SUV, using a point source and a uniform phantom to obtain

the sensitivity and volume sensitivity factors. These factors are specific to the radionuclide and collimator type. Consequently, SPECT images acquired using the OSCGM reconstruction method show the radioactivity concentration, making it possible to evaluate quantitative data.

Data analysis

CT, μ -map, and SPECT images with varying CT collimation width and slice thickness were analyzed by the following methods.

The FWHM of the slice sensitivity profile (SSP) on CT images of the micro-coin phantom were measured using CTmeasure Ver. 0.97b (Japanese Society of CT Technology, Tokyo, Japan) (11) and the z-axis (i.e., axial) resolution was evaluated. Measurements were performed 5 times and the results are shown as means.

SPECT/CT images of the NEMA body phantom were analyzed using a measuring application (Volumetric Analysis; Siemens Healthcare). Circular regions of interest (ROIs) were drawn on six spheres in the slice best depicting the 17-mm-diameter sphere by referring to the CT images. In addition, the same circular ROIs as the 17-mm-diameter sphere were drawn on 12 BGs in 5 consecutive slices next to the same slice as above. Figure 1b shows an example of the drawn ROIs.

The standard deviation (SD) of the CT values (Hounsfield units) in the ROIs on BG was measured to assess noise in the CT images. Subsequently, the mean CT values and the SD in the ROIs on a 17 mm sphere were measured. Similarly, the mean and the SD of the linear attenuation coefficient in the ROIs on a 17-mm-diameter sphere of the μ -map images were measured using a measuring application (Series ROI and Curve; Siemens Healthcare).

Additionally, the volume CT dose index (CTDI_{vol}) and dose length product (DLP) displayed on the system after the CT scans of the NEMA body phantom along with their relative ratios based on a collimation width of 2.0 mm were investigated to evaluate the radiation dose.

The mean SPECT values and the SD of the ROIs on the six spheres and the BG were measured, and the percentage contrast (Q_H) and background variability (N_B) were calculated using the following formula to evaluate the SPECT image quality (12).

$$Q_{H,17mm} = \frac{C_{H,17mm}/C_{B,17mm} - 1}{A_H/A_B - 1} \times 100 (\%)$$

$$N_{B,17mm} = \frac{SD_{B,17mm}}{C_{B,17mm}} \times 100 (\%)$$

Then, the absolute recovery coefficient (ARC) was calculated from the following formula to assess the quantitative accuracy of the SPECT image.

$$ARC = \frac{C_{H,10-37mm}}{A_H}$$

A_H and C_H represent the absolute activity concentration and the mean SPECT values (Bq/ml) in the ROIs on the spheres, respectively, and A_B and C_B represent the corresponding values in the ROIs on the BG. SD_B represents the SD (Bq/ml) in the ROIs on BG.

Clinical cases

The radiation doses of CT scans in 77 consecutive patients (72 men and 5 women; mean age \pm SD, 72.9 \pm 10.3 years [range, 32-94 years]; mean body mass index (BMI) \pm SD, 23.2 \pm 3.4 kg/m² [range, 17.2-35.6 kg/m²]) were retrospectively reviewed. All patients underwent bone SPECT and accompanying chest and abdominopelvic CT at Chiba Aoba Municipal Hospital between April 1, 2019 and February 28, 2020. CT scans were acquired with a tube voltage of 130 kVp, gantry rotation time of 0.6 s, 60 reference mAs using an automatic exposure control system (CARE Dose 4D), pitch factor of 1.8, FOV of 500 mm, and collimation of 6 \times 2.0. Accordingly, the radiation doses were as follows: effective mAs, 40.4 \pm 9.0; CTDI_{vol}, 4.5 \pm 1.0 mGy; and DLP, 359.5 \pm 85.5 mGy-cm.

Of the above patients, 23 (22 men and 1 woman; mean age \pm SD, 71.3 \pm 18.4 years [range, 56-94 years]; mean BMI \pm SD, 21.5 \pm 5.4 kg/m² [range, 17.2-27.1 kg/m²]) diagnosed by radiologists were classified into 3 groups (normal lumbar spine, thoracolumbar spine with suspected bone metastasis, and hip bone with suspected bone metastasis) and retrospectively analyzed. The clinical bone SPECT procedure was

performed according to the routine clinical practice at our institution; SPECT scans were performed 3.5 h after intravenous administration of 22.5 \pm 5.1 mCi (832.2 \pm 187.6 MBq) of ^{99m}Tc-methylene diphosphonate (^{99m}Tc-MDP) using the same parameters as in the phantom study, followed by the above chest and abdominopelvic CT scans. SPECT reconstruction was performed using 1 subset and 48 iterations and a Gaussian filter with a FWHM of 10.0 mm; all other parameters were the same as in the phantom studies. CT data were generated with slice thicknesses of 4.0, 8.0, and 10.0 mm due to a collimation width of 3.0 mm, and a slice gap equal to the slice thickness, using a filter kernel (B31s medium smooth).

ROIs were drawn on the same slice, determined visually and transformed using the same threshold (50%) of the mean SPECT values for all SPECT images by the application Volumetric Analysis. Image analysis was performed by a single radiological technologist. The relative ratios of the mean SPECT values and SD of SPECT values at different CT slice thicknesses, which were based on 8.0 mm, were calculated by the following formulas, and are shown as means and SD in each patient group.

$$\text{Relative ratio of the mean SPECT values} = \frac{\text{Mean SPECT values}_{4.0,8.0,10.0 \text{ mm}}}{\text{Mean SPECT values}_{8.0 \text{ mm}}}$$

$$\text{Relative ratio of SD of SPECT values} = \frac{\text{SD of SPECT values}_{4.0,8.0,10.0 \text{ mm}}}{\text{SD of SPECT values}_{8.0 \text{ mm}}}$$

Furthermore, the Steel-Dwass test was used to statistically analyze differences in the mean SPECT values and the SD of SPECT values due to the CT slice thickness in all groups. The analysis was performed using EZR software (Saitama Medical Center, Jichi Medical University, Saitama, Japan), a graphical user interface for R. A P-value of less than 0.05 was considered statistically significant.

Results

CT and μ -map image with varied CT parameters

As the CT collimation width and reconstruction slice thickness were increased, the FWHM of the SSP tended to increase. When the reconstruction slice thickness was decreased and approached the collimation width, it deviated from the FWHM (e.g., FWHM was 2.13 mm when the collimation width was 1.0 mm and the slice thickness was 1.25 mm). A slice thickness 2.5 to 3 times the collimator width was approximated to the FWHM (e.g., FWHM was 5.24 mm when the collimation width was 2.0 mm and the slice thickness was 5.0 mm). The FWHM of the SSP is presented in Table 1.

As the slice thickness was increased, the SD of the BG in CT images decreased. Similarly, The SD of CT images decreased as the collimation increased, but the decrease was slight for slice

thicknesses of 8.0 mm and 10 mm. Figure 2 shows the SD of the BG in CT images.

Table 1. FWHM of the SSP on CT images with varying collimation width and slice thickness

		FWHM (mm)							
							Thickness (mm)		
Collimation (mm)		1.25	2.5	3.0	4.0	5.0	6.0	8.0	10.0
1.0		2.13	2.62	2.94	3.87	4.81	6.07	7.91	9.74
2.0		—	4.11	4.14	5.22	5.24	5.88	7.77	9.71
3.0		—	—	—	6.03	6.07	7.25	8.21	9.69

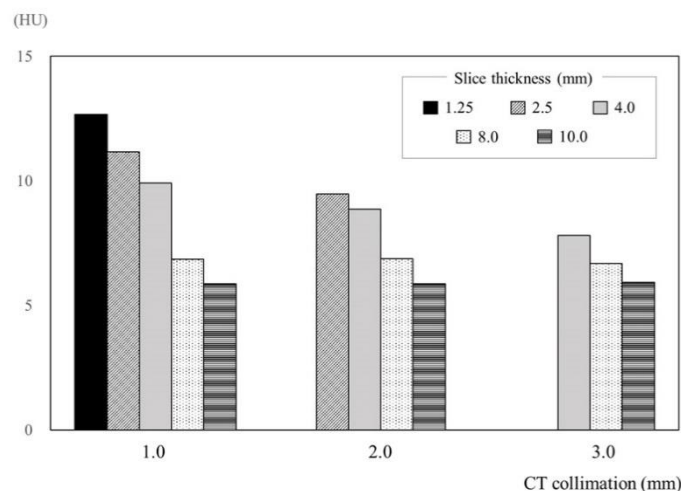


Figure 2. SD of the BG in CT images with varying collimation width and slice thickness
HU, Hounsfield units

The mean CT values and the SD of the 17-mm-diameter sphere in the CT images changed when the collimation width and slice thickness changed, but the mean and SD of the linear attenuation coefficient of the 17-mm-diameter sphere of the μ -map images showed no change. These results are presented in Table 2.

The relative ratios of CTDIvol (mGy) based on a CT collimation width of 2.0 mm which is used

clinically, were as follows: collimation width of 1.0 mm, 1.17; 3.0 mm, 0.94. Similarly, the relative ratios of DLP (mGy*cm) based on the CT collimation width of 2.0 mm were as follows: collimation width of 1.0 mm, 1.10; 3.0 mm, 0.99. CTDIvol and DLP decreased as the collimation width was increased. Table 3 presents CTDIvol, DLP, and their relative ratios.

Table 2. Mean CT values and SD in CT images, and mean and SD of the linear attenuation coefficient in the μ -map images with varying collimation width and slice thickness of CT

		Mean CT values (HU)					Mean linear attenuation coefficient (cm ⁻¹)					
		Thickness (mm)					Thickness (mm)					
Collimation (mm)		1.25	2.5	4.0	8.0	10.0	Collimation (mm)	1.25	2.5	4.0	8.0	10.0
1.0		18.6	16.9	17.9	33.8	27.3	1.0	0.16	0.16	0.16	0.16	0.16
2.0		—	20.4	17.5	29.5	28.0	2.0	—	0.16	0.16	0.16	0.16
3.0		—	—	19.7	32.6	24.5	3.0	—	—	0.16	0.16	0.16

		SD of CT values (HU)					SD of linear attenuation coefficient (cm ⁻¹)					
		Thickness (mm)					Thickness (mm)					
Collimation (mm)		1.25	2.5	4.0	8.0	10.0	Collimation (mm)	1.25	2.5	4.0	8.0	10.0
1.0		33.0	33.9	34.5	24.4	27.6	1.0	0	0	0	0	0
2.0		—	34.4	33.6	23.7	27.2	2.0	—	0	0	0	0
3.0		—	—	32.4	21.5	29.3	3.0	—	—	0	0	0

ROIs were drawn on an image of a 17-mm-diameter sphere in a NEMA body phantom

Table 3. CTDIvol and DLP with CT collimation widths of 1.0 mm, 2.0 mm, 3.0 mm, and their relative ratios compared to a collimation width of 2.0 mm

Collimation (mm)	CTDIvol (mGy)	Relative ratio	DLP (mGy·cm)	Relative ratio
1.0	5.08	1.17	119.4	1.10
2.0	4.36	1.00	109.0	1.00
3.0	4.08	0.94	107.7	0.99

SPECT image with varied CT parameters

Both Q_H and N_B on the SPECT images did not change, even when the CT collimation width and slice thickness were varied. Figure 3a and b show Q_H and N_B , respectively. ARC also showed

no change when the CT collimation width and slice thickness were varied. Moreover, ARC improved as the diameter of the ROI grew. The ARC is shown in Figure 4.

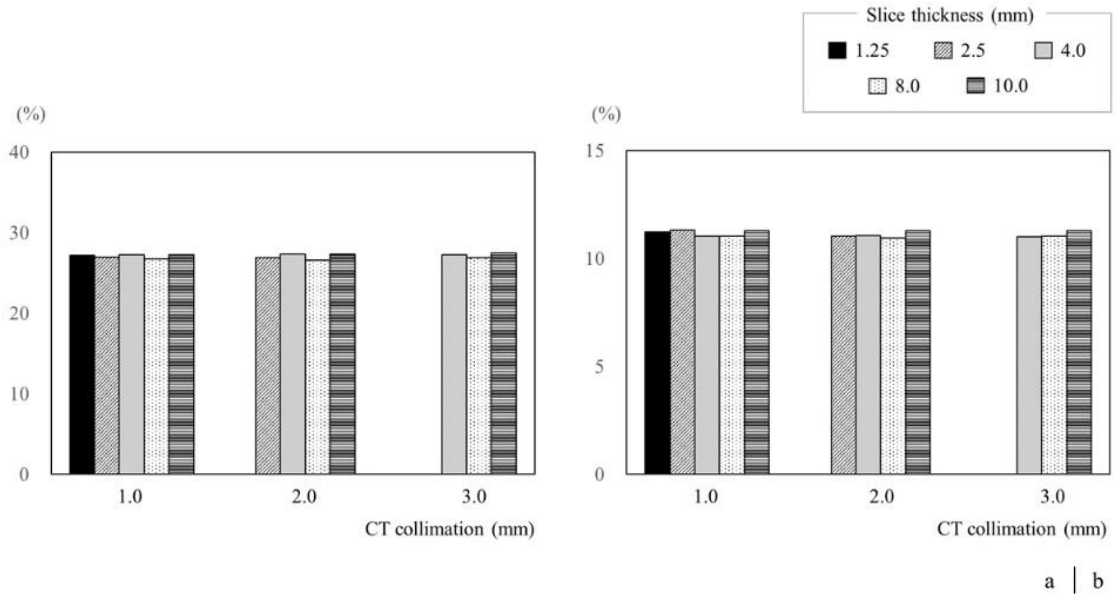


Figure 3. (a) Percentage contrast and (b) background variability with varying CT collimation width and slice thickness

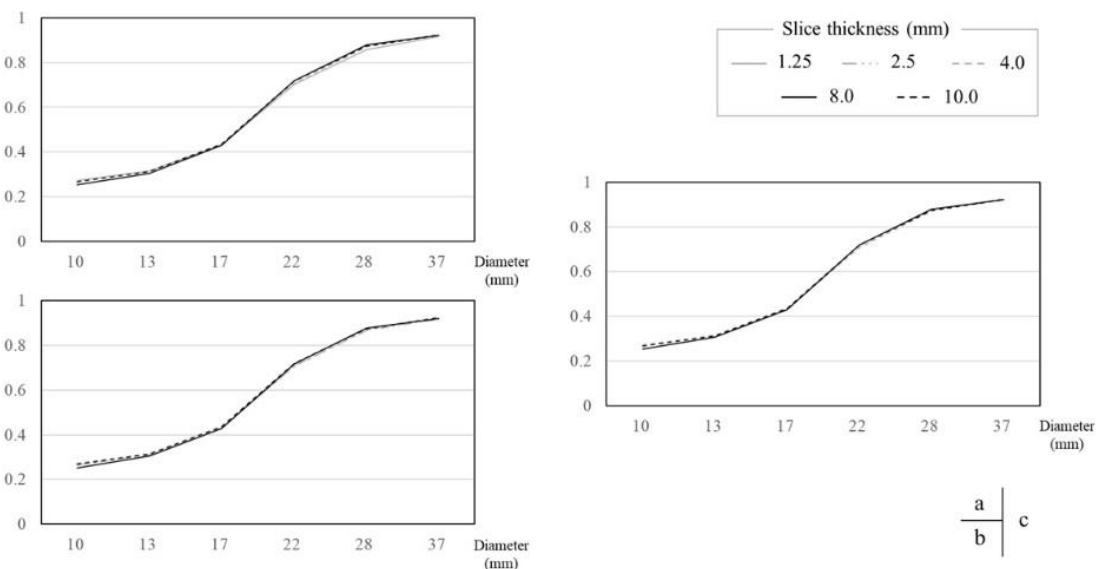


Figure 4. Absolute recovery coefficient calculated from mean SPECT values with varying CT slice thickness and collimation width of (a) 1.0 mm, (b) 2.0 mm, and (c) 3.0 mm

In addition, CT, μ -map, and SPECT images of the NEMA body phantom are shown in Figure 5. The CT image noise of the BG and the six

spheres was visibly different depending on the CT slice thickness: the thicker the slice, the smoother the CT image. Nevertheless, by

conversion to the μ -map image, the differences in the image noise became less noticeable. Additionally, there were no visual difference in

the SPECT image noise. The SD of the BG activity measured in the process of calculating N_B were 2.138-2.230 (mean, 2.181; SD, 0.028).

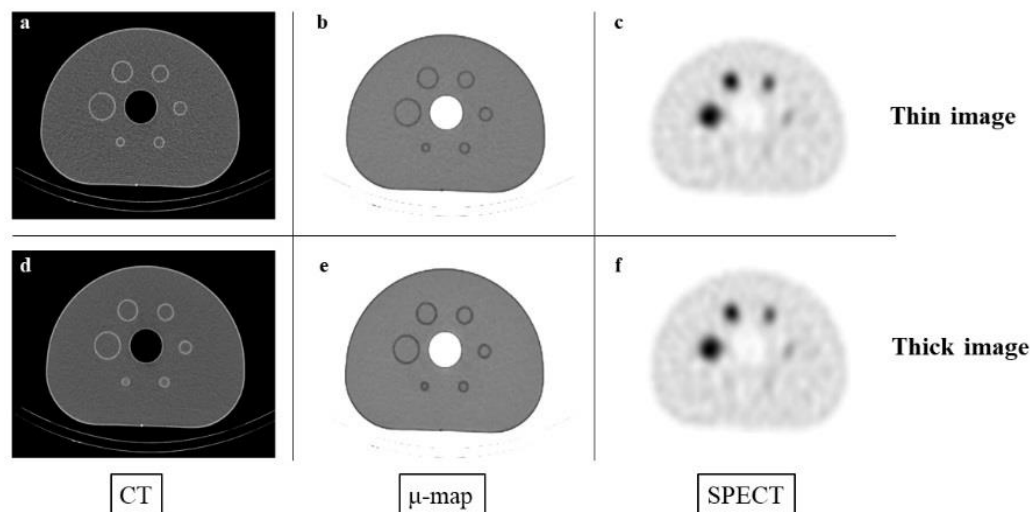


Figure 5. (a, d) CT, (b, e) μ -map, and (c, f) SPECT images of the NEMA body phantom with varying CT parameters. (a, b, c) CT images with the thinnest collimation width of 1.0 mm and slice thickness of 1.25 mm, and (d, e, f) CT images with the thickest collimation width of 3.0 mm and slice thickness of 10.0 mm, which were used for attenuation correction and image reconstruction

Validation of clinical images

The relative ratios representing the mean in each patient group were as follows: mean SPECT values on a CT slice thickness of 4.0 mm, 0.98-1.02 (SD, 0.98-0.99); mean SPECT values on a CT slice thickness of 10.0 mm, 0.97-1.02 (SD, 0.98-1.03). The relative ratios representing the SD in each patient group were as follows: mean SPECT values on a CT slice thickness of 4.0 mm, 0.04-0.07 (SD, 0.03-0.08); mean SPECT values on a CT slice thickness of 10.0 mm, 0.04

- 0.07 (SD, 0.04 - 0.05). These results showed no notable differences in mean SPECT values in clinical SPECT images resulting from changes in CT slice thickness and individual differences, and the SD of the SPECT values was small. Furthermore, there were no statistically significant differences in the mean SPECT values and the SD values resulting from differences in CT slice thickness. Table 4 presents the image analysis results for clinical cases.

Table 4. Relative ratios of mean SPECT values and SD based on a CT collimation width of 8.0 mm with varying CT slice thickness in the clinical cases (shown as mean \pm SD in each patient group)

Case	Normal third lumbar vertebra		Thoracolumbar spine with suspected bone metastasis		Hip bone with suspected bone metastasis		Statistical test	
	Mean (Bq/ml)	SD (Bq/ml)	Mean (Bq/ml)	SD (Bq/ml)	Mean	SD	Mean	SD
4 mm	1.00 \pm 0.07	0.99 \pm 0.08	0.98 \pm 0.07					
8 mm	1.00	1.00	1.00					
10 mm	1.02 \pm 0.04	1.03 \pm 0.05	0.97 \pm 0.07					

n.s.: not significant
 ROIs were drawn on images for the following groups: normal third lumbar vertebra, thoracolumbar spine with suspected bone metastasis, and hip bone with suspected bone metastasis.
 The Steel-Dwass test was used for comparison in all cases

Discussion

In this study, we investigated SPECT/CT imaging because it was suspected that the image reconstruction method in which SPECT images are arranged according to the CT coordinate system would be influenced by the CT parameters, which might alter the SPECT images. As shown in Table 1, as the collimation width and slice thickness were increased, the FWHM of the SSP on CT images tended to increase. Moreover, the FWHM for a small slice thickness closer to the collimation width deviated considerably from the thickness setting, effectively representing the z-axis resolution. We speculate that this observation was due to the simple helical reconstruction method used for image reconstruction, and due to the coarse sampling of z-axis data with a large pitch factor of 1.8, which significantly increased the FWHM. It has been reported that this issue can be mitigated by applying a tilted-plane Feldkamp-type reconstruction algorithm (13); however, this was not implemented in the SPECT/CT system in this study. Meanwhile, although the data are not shown here, it was verified that the FWHM improved and moved closer to the thickness setting as the pitch factor was decreased (14). However, because of the maximum of 6 CT slice acquisitions per rotation by the SPECT/CT system and because imaging is generally performed while the patient holds their breath, it is not realistic to reduce the pitch factor in clinical practice. It also must be considered that CTDIvol and DLP increases as the pitch factor is decreased. Although dependent on the size of the patient, it takes about 20 s for CT imaging of the trunk even if the pitch factor is 1.8.

The SD of the BG in CT images, which represents image noise, decreased with increasing collimation width and slice thickness (Figure 2). When the slice thickness was large, the decrease in SD was slight even when the collimation width was increased. We speculate that this observation was due to the FWHM of the SSP remaining the same regardless of the collimation width when slice thickness was increased.

As shown in Table 2, although the mean CT values and SD in CT images changed according to the collimation width and slice thickness, the mean and SD of the linear attenuation coefficient in the μ -map images did not change, even for the same target. We speculate that the effects of collimation width and slice thickness were reduced in the process of converting CT images to μ -map images. In addition, given that a smoothing filter was not applied to the CT images used for OSCGM algorithm, we presume

that the abovementioned effects are not the result of smoothing the distribution of the linear attenuation coefficient by the filter.

However, we consider that CTDIvol and DLP decreased as the collimation width was increased because the radiation dose utilization efficiency improved (Table 3) (15). Conversely, there was a relative increase in radiation dose with a CT collimation width of 1.0 mm. This observation may explain why applying a thick collimation width is recommended for reducing the radiation dose, except in cases where high z-axis resolution of CT images is required.

As shown in Figure 3, there was no change in the Q_H and N_B of the SPECT image due to changes in CT collimation width and slice thickness. Likewise, ARC did not change according to CT collimation width or slice thickness (Figure 4). That is, SPECT image quality and quantitative accuracy were not affected by these CT parameters. As described above, even when the CT values varied, these changes were mitigated by the conversion to the μ -map; therefore, we considered that SPECT images using a μ -map image for attenuation correction also did not fluctuate significantly. This observation was also consistent with visual evaluation of the images in Figure 5. Furthermore, the increase in ARC with larger ROI diameters was caused by a reduction of partial volume effects due to the low resolution and consequently larger mean SPECT values (16).

Given that the NEMA body phantom has simple structures, we presumed that the distribution of the linear attenuation coefficient of the γ -rays would differ from that of the human body, with its vastly more complicated structures and shape that differs along the z-axis. Consequently, we conducted an image analysis in clinical cases. Even when the CT collimation width and slice thickness were varied, the mean SPECT values and SD did not vary, and there were no statistically significant differences (Table 4). Individual differences were also not observed. Similar to the phantom, the μ -map image of the human body, which has complicated radiation attenuation, was less affected by the CT parameters, and it seems that the SPECT image was not affected either.

Both fused images and independent CT images are used for clinical diagnosis when performing SPECT/CT examinations at our institution. However, a high number of false-positive incidental findings have been detected on CT images produced for attenuation correction of SPECT images (17). It is important to set the slice thickness and CT dose by considering the z-axis resolution and image noise according to the purpose of the examination when providing

independent CT images in clinical practice. In cases where high z-axis resolution is not required, applying a thick collimation width or slice thickness can reduce the radiation dose or image noise. The findings of this study suggest that it is essential to devise appropriate CT parameter settings for SPECT/CT and that the SPECT images were not affected.

Limitation

This study was performed using a fixed subset and iterations, without using zone-map enhancement, which improves the image quality of SPECT images reconstructed with the addition of tissue division information from CT images (18). Therefore, it is possible that different results would have been obtained if the parameter settings had been changed. In addition, the z-axis resolution of SPECT images was not evaluated. It may be necessary to evaluate it in the future.

Conclusion

Varying the CT collimation width and slice thickness had no effect on SPECT image quality and quantitative accuracy, but CT image noise, z-axis resolution, and radiation dose were affected.

Ethical approval and consent to participate

This study was conducted under the approval of the Ethics Committee of Chiba Aoba Municipal Hospital. All procedures performed in studies involving human participants were in accordance with the 1964 Helsinki declaration and its later amendments or comparable ethical standards.

The requirement of obtaining informed consent was waived by our ethics committee due to the anonymization of personal information and the retrospective nature of the study.

Conflict of interest

The authors have no conflicts of interest to declare.

References

- Lucignani G, Paganelli G, Bombardieri E. The use of standardized uptake values for assessing FDG uptake with PET in oncology: A clinical perspective. *Nuclear Medicine Communications*. 2004; 25 (7): 651–656.
- Dale L, Bailey, Kathy P, Willowson. An Evidence-Based Review of Quantitative SPECT Imaging and Potential Clinical Applications. *J Nucl Med*. 2013; 54 (1): 83-89.
- Kuji I, Yamane T, Seto A, Yasumizu Y, Shirotake S, Oyama M. Skeletal standardized uptake values obtained by quantitative SPECT/CT as an osteoblastic biomarker for the discrimination of active bone metastasis in prostate cancer. *Eur J Hybrid Imaging*. 2017; 1(1): 2.
- Burger C, Goerres G, Schoenes S, Buck A, Lonn AH, Von Schulthess GK. PET attenuation coefficients from CT images: experimental evaluation of the transformation of CT into PET 511keV attenuation coefficients. *Eur J Nucl Med Mol Imaging*. 2002; 29(7): 922-927.
- Bailey DL, Willowson KP. An evidence-based review of quantitative SPECT imaging and potential clinical applications. *J Nucl Med*. 2013; 54(1): 83-89.
- Monzen Y, Tamura A, Okazaki H, Kurose T, Kobayashi M, Kuraoka M. SPECT/CT Fusion in the Diagnosis of Hyperparathyroidism. *Asia Ocean J Nucl Med Biol*. 2015; 3(1): 61–65.
- Vija AH. Introduction to x SPECT Technology: Evolving Multi-modal SPECT to Become Context-based and Quantitative. White paper 2013. https://static.healthcare.siemens.com/siemens_hwem-hwem_sxxa_websites-context-root/wcm/idc/groups/public/@global/@imaging/@molecular/documents/download/mdax/otiz/~edisp/final_new_xspect_wp.2-00960488.pdf (Accessed 2020.05.10)
- Okuda K, Sakimoto S, Fujii S, Ida T, Moriyama S. Influence of the Pixel Sizes of Reference Computed Tomography on Single-photon Emission Computed Tomography Image Reconstruction Using Conjugate-gradient Algorithm. *Nihon Hoshasen Gijutsu Gakkai Zasshi*. 2017; 73(10):1039-1044.
- Goto M, Tominaga C, Taura M, Azumi H, Sato K, Homma N, et al. A method to measure slice sensitivity profiles of CT images under low-contrast and high-noise conditions. *Phys Med*. 2019; 60: 100-110.
- Nakahara T, Daisaki H, Yamamoto Y, Iimori T, Miyagawa K, Okamoto T, et al. Use of a digital phantom developed by QIBA for harmonizing SUVs obtained from the state-of-the-art SPECT/CT systems: a multicenter study. *EJNMMI Res*. 2017; 7(1): 53.
- Ichikawa K. CTmeasure. Japanese society of CT technology. 2012-2014. <http://www.jsct-tech.org/> (Accessed 2020. 05.10).
- National Electrical Manufacturers Association. Performance measurements of positron emission tomographs. NEMA Standards Publication NU 2-2012. Rosslyn: National Electrical Manufacturers Asso-

- ciation; 2012. <http://dea.unsj.edu.ar/mednuclear/PET-NEMA-NU2-2001.pdf>. Accessed 22 Dec 2020.
13. Yan M, Zhang C. Tilted plane Feldkamp type reconstruction algorithm for spiral cone beam CT. *Med Phys* 2005; 32(11): 3455-67.
 14. Mackie A, Hart GC, Williams-Butt JF. Ramp test objects for slice sensitivity profile measurement in spiral CT. *Br J Radiol* 1997; 70(837): 942-945.
 15. Perisinakis K, Papadakis AE, Damilakis J. The effect of x-ray beam quality and geometry on radiation utilization efficiency in multidetector CT imaging. *Med Phys* 2009; 36(4):1258-1266.
 16. Zito F, Gilardi MC, Magnani P, Fazio F. Single-photon emission tomographic quantification in spherical objects: effects of object size and background. *Eur J Nucl Med*. 1996; 23(3):263-271.
 17. Coward J, Nightingale J, Hogg P. The Clinical Dilemma of Incidental Findings on the Low-Resolution CT Images from SPECT/CT MPI Studies. *J Nucl Med Technol*. 2016; 44(3): 167-172.
 18. Okuda K, Fujii S, Sakimoto S. Impact of Novel Incorporation of CT-based Segment Mapping into a Conjugated Gradient Algorithm on Bone SPECT Imaging: Fundamental Characteristics of a Context-specific Reconstruction Method. *Asia Ocean J Nucl Med Biol*. 2019; 7(1):49-57.